Automated Stereophotogrammetry Data Cleansing

Stuart Henry, Philip Morrow, John Winder, and Bryan Scotney

Abstract—The stereophotogrammetry modality is gaining more widespread use in the clinical setting. Registration and visualization of this data, in conjunction with conventional 3D volumetric image modalities, provides virtual human data with textured soft tissue and internal anatomical and structural information. In this investigation computed tomography (CT) and stereophotogrammetry data is acquired from 4 anatomical phantoms and registered using the trimmed iterative closest point (TrICP) algorithm.

This paper fully addresses the issue of imaging artifacts around the stereophotogrammetry surface edge using the registered CT data as a reference. Several iterative algorithms are implemented to automatically identify and remove stereophotogrammetry surface edge outliers, improving the overall visualization of the combined stereophotogrammetry and CT data. This paper shows that outliers at the surface edge of stereophotogrammetry data can be successfully removed automatically.

Keywords—Data cleansing, stereophotogrammetry.

I. INTRODUCTION

THE diagnosis and treatment planning of patients with specific diseases requires image data acquisition from a range of volumetric modalities including computed tomography (CT), magnetic resonance (MR), single photon emission tomography (SPECT) and positron-emission tomography (PET) [1]. Image registration is used to spatially align multi-modal image data, combining both anatomical and functional information, whilst reducing the weaknesses of the modalities involved [2]. These modalities provide excellent structural and functional information but produce no textural information relating to the surface texture of the skin.

Stereophotogrammetry is a 3D surface imaging modality that produces high resolution topographical surface maps with surface texture information. Capture of 3D stereophotogrammetry data involves the acquisition of images from two or more pairs of stereoscopic cameras, acquiring data from different viewpoints. The 3D location of a point in the surface is calculated by locating this point in each of the acquired stereoscopic image. From this information, the geometry of the cameras and triangulation is used to determine this points location in 3D space [3]. Stereophotogrammetry is gaining more widespread popularity in the clinical setting as a result of an increase in the systems available commercially [4]. Combining the stereophotogrammetry data with data from conventional medical imaging modalities (CT and MR), has the potential to provide a better visualization on how soft tissue surface disease relates to the internal anatomy of the patient. Previous applications of combining this data have been in the planning and post operative evaluation of maxillofacial surgery and in the evaluation of cadavers in forensic medicine [5], [6].

Although stereophotogrammetry does not provide internal anatomical data, there are many benefits associated with using this modality in the clinical setting. These benefits include short acquisition time (0.002s); demonstrated accuracy of 0.5mm in each orthogonal axes; easy calibration; non invasiveness; no requirement for injected tracers; no moving parts; and inexpensive hardware [7], [8]. Since patients are not exposed to potentially harmful radiation, unlike CT imaging, stereophotogrammetry can be used for follow up assessment without having to consider patient safety. Furthermore this modality is well suited for follow up data acquisition over time since as it can shows the effect of internal structural change to the soft tissue surface.

The area around the stereophotogrammetry surface edge is prone to imaging artifacts, considered as outliers due to these regions being near the limits of the camera's field of view. Such outlier regions can create a misrepresentation of these areas with the potential to cause misinterpretation of the stereophotogrammetry surface data. Therefore in combining 3D surface texture from stereophotogrammetry with 3D volumetric image data, careful consideration is required in choosing an outlier robust registration algorithm.

The focus of this paper is to address the problem of surface edge outliers in the stereophotogrammetry data and demonstrate how these outliers may be removed automatically. The aim of this paper is to improve the overall visualization of registered stereophotogrammetry and CT data. To achieve this, several iterative automated cleansing algorithms have been developed and implemented to identify and remove surface edge outliers.

II. METHODOLOGY

A. Image Acquisition

In this investigation four anatomical phantoms were selected for data acquisition from both stereophotogrammetry

Stuart Henry is a PhD student within the School of Computing and Information Engineering at the University of Ulster, UK (phone: +44 28 7012 4698; e-mail: henry-r3@email.ulster.ac.uk).

Dr. Philip Morrow is a Reader within the Computer Science Research Institute at the University of Ulster, UK (phone: +44 28 70124637; email: pj.morrow@ulster.ac.uk).

Dr. John Winder is a Lecturer in Clinical Physiology within the Institute of Nursing Research at the University of Ulster, UK (phone: +44 28 90368440 email: rj.winder@ulster.ac.uk).

Prof. Bryan Scotney is the Director of the Computer Science Research Institute at the University of Ulster, UK (phone: +44 28 70124648 email: bw.scotney@ulster.ac.uk).

and CT modalities. The four phantoms selected were a mannequin head model made from polystyrene; a plastic radiography head model used for teaching with 12 traverse slices and bone inside; a right foot molded in Perspex with bone inside; and a silicone based right foot with 3 simulated ulcers on the surface (Fig. 1). These phantoms were selected as the acquired data from them produces different types of artifacts with complex curved surfaces in clinically valid anatomical regions.

Fig. 1 The four anatomical phantoms used in this investigation (a) polystyrene head mannequin model; (b) plastic radiography head model with 12 traverse slices; (c) a Perspex foot with bone encapsulated; (d) silicone based foot with 3 simulated ulcers

The stereophotogrammetry data was acquired using the Di3D passive stereophotogrammetry system (Dimensional Imaging, Glasgow, UK, www.di3d.com). This system has two pairs of Canon EOS 1000D 10.1 Megapixel cameras, each with 18-55mm wide angle zoom lenses. For each camera pair a synchronized SunPak 383 Autoflash is attached (Fig. 2). The data provided by the camera system is inputted into the manufacturers software, Di3dCapture (version 5.2.5), to capture and build the 3D textured surface. Prior to data acquisition the Di3D system was calibrated. The 3D phantom was placed at a distance of 90cm from the centre of the system and data captured with shutter speed 50ms, ISO speed 100 and a flash brightness of ¼ in accordance with the manufacturers recommended settings.

Fig. 2 The Di3D stereophotogrammetry system connected to the laptop with Di3dCapture installed

The CT data was acquired from a Philips Brilliance 10 Slice System CT scanner with a slice thickness of 1mm (www.philipsctscanner.com/ct-scanner/) in the Digital Imaging and Communications in Medicine (DICOM) format. The scanner bed was removed from the CT manually and the surface phantom rendered using the marching cubes algorithm within the Mayo Clinic Analyze® 10.0 imaging software (Mayo Clinic, Rochester, USA, (http://www.mayo.edu/bir/Software/Analyze/Analyze.html)

[9], [10]. Surface image data from both modalities was stored in the Wavefront Object file format [11]. Prior to registration surface data from both modalities was decimated to 10% of their original facets using a quadratic edge collapse decimation with a quality threshold of 0.5 within Meshlab (version 1.3.1) [12].

B. Image Registration

In this investigation the stereophotogrammetry data is registered with the CT data, using the registration between the two surfaces to identify outliers in the stereophotogrammetry data. The outlier robust Trimmed iterative closest point (TrICP) algorithm by Chetverikov, Steapnov and Krsek is used to register the stereophotogrammetry surface to the CT surface [13]. The TrICP algorithm is a variant of the commonly used iterative closest point algorithm, which is successful in registering partially overlapping 3D point sets that have shape defects and outliers present in the surfaces. TrICP uses the least trimmed squares of corresponding point distances between the two surfaces, to classify and exclude outliers at each iteration. A previous investigation has shown that TrICP is very robust in the presence of high levels of Gaussian and impulsive noise, so is suited to accurately registering surface data with artifacts present [14].

Prior to the registration, the stereophotogrammetry surface was manually moved to within 30° of the CT data. This was necessary since the TrICP algorithm requires the two surfaces to be within 30° of each other prior to registration [13]. Using the TrICP algorithm the stereophotogrammetry surface was registered to the CT surface.

The TrICP algorithm was implemented in Matlab R2012a with a k-d tree in C++. The termination conditions for the TrICP algorithm were:

1. The maximum number of 300 iterations was exceeded. This value was selected to give TrICP sufficient iterations for convergence
2. The change in error measure between iterations was less than 1×10^{-5}mm.

The TrICP algorithm produced a transformation matrix which was applied to the stereophotogrammetry OBJ file so that it was in spatial correspondence with the CT OBJ surface.

C. Stereophotogrammetry Surface Edge Outlier Problem

To demonstrate that the stereophotogrammetry surface edge suffers from artifacts and outliers, the registration of this surface with the CT surface is used. Surfaces from both modalities are represented as triangular meshes where the stereophotogrammetry surface is a sub surface of the CT surface. The CT surface is used as a reference model and for each stereophotogrammetry surface node the closest node in the CT surface is found using a k-d tree. The nodes on the stereophotogrammetry surface edge were located. Distribution of the corresponding distances between each stereophotogrammetry surface node and its closest CT node was calculated. Also the distribution of corresponding distances for all the stereophotogrammetry surface edge nodes was generated (Fig. 3). By removing surface edge levels 1-3, Fig. 3, a distribution of corresponding distances was calculated, displaying the impact of removing this potentially

erroneous data from around the surface edge. Using the sub surface representation in Fig. 3, where nodes 1-6 in level 1, nodes 7-12 in level 2 and nodes 13-17 in level 3 are removed, the corresponding distance distribution of the remaining stereophotogrammetry surface nodes can be calculated. The corresponding node distances were placed in bins with a corresponding distance of size 0.5mm, with the frequency and normalized frequency distributions of these distances found. The issue of outliers on the stereophotogrammetry edge can be displayed by plotting these normalized distributions and comparing the proportion of outliers nodes for the entire surface, the surface edge and the remaining nodes (with surface edge levels 1-3 removed).
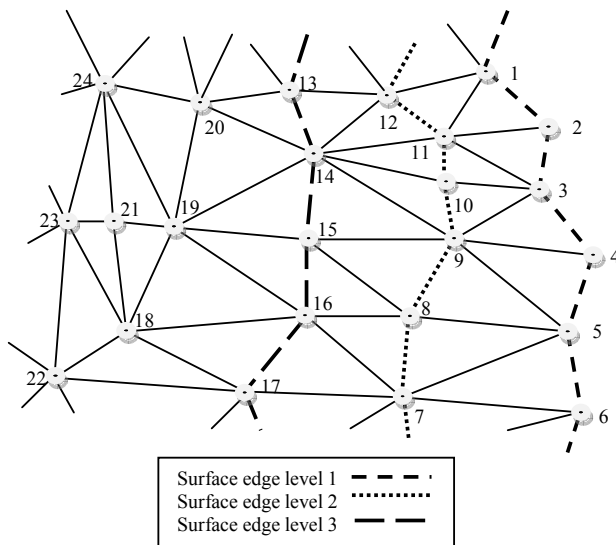

Fig. 3 A partial surface mesh depicting the surface edge levels; level 1 nodes (1 – 6); level 2 nodes (7-12); level 3 nodes (13-17)

The normalized distribution of corresponding node distances for the plastic head data in Fig. 4(a) shows that the surface edge nodes have a wider corresponding distribution in comparison with the distribution for the entire surface nodes. The corresponding distances for the entire surface has 86.98% of the nodes with a corresponding distance of <2.5mm, compared with 61.85% for the surface edge and 91.50% for the remaining surface nodes. This implies that most of the outliers lie on the surface edge, and by removing surface edge levels 1-3, the proportion surface nodes in this range can be improved. Removing surface edge levels 1-3 generates a distribution that converges to 0% at 7mm compared with the normalized distribution for all the surface nodes converging to 0% at 8mm. Further evidence of outliers on the surface edge can be seen on the normalized surface edge distribution as it converges to 0% at a large corresponding distance and the small peak at 6-7mm.

Further evidence of the surface edge outlier problem is shown in the normalized distribution of corresponding node distances for the remaining phantoms. In the normalized distributions for the polystyrene head data, the distribution of the corresponding distances for the entire surface converges to 0% at 7mm shown in Fig. 4(b). Removal of the nodes in surface edge levels 1-3 improves to convergence to 0% at

5mm. With the silicone foot data the normalized distribution of corresponding distances is improved (Fig. 4(c)). The normalized distribution converges to 0% at 12mm with all the surface nodes, compared with a convergence at 9mm for the surface nodes with surface edge levels 1-3 removed. The stereophotogrammetry data for the Perspex foot has a large artifact in the ankle region. The surface edge outliers have a maximum distribution of 11.74% at 1mm (Fig. (d)). This is a lower maximum distribution of nodes compared with the entire surface, 20.73%. Removal of surface edge levels 1-3 improves the maximum distribution at 1mm to 22.92%, showing that the surface edge has a lot of outlier data present.

From the analysis of the stereophotogrammetry surface edge distances, it is clearly demonstrated that the there is a higher proportion of outliers at the surface edge compared with the entire surface. By removing the areas around the surface edge, the overall corresponding node distribution can be improved and the proportion of large distances is either removed or lowered. An automated cleansing algorithm to detect and remove these stereophotogrammetry surface edge outliers would potentially improve the visualization with the registered CT surface. This cleansing would aid clinicians as erroneous data in these regions would be removed, providing a more accurate digital human representation. Automated cleansing would remove the requirement for manual cleansing interventions which can be time consuming and operator dependent.

D. Automated Data Cleansing Algorithms

To automatically cleanse the stereophotogrammetry surface, by detecting and removing outliers on the surface edge, the CT surface is used as a reference model, with the closest corresponding node in the CT surface located for each stereophotogrammetry node. Several automated cleansing approaches are proposed, which use the corresponding node distances between the registered stereophotogrammetry surface and CT surface to determine a distance threshold. This distance threshold will determine which nodes on the stereophotogrammetry surface edge can be determined as outliers and subsequently removed from the surface.

1) Otsu's Method

The first approach investigated was Otsu's method, a frequently used automatic thresholding detection mechanism in image segmentation to determine thresholds for partitioning images into regions depending on their intensity values [15]. This method maximizes the between-class variance or corresponding node distance creating two separate classes which are a class of surface nodes deemed as inliers and a second class of surface nodes that have been identified as outliers. The two classes created by Otsu's thresholding are distinct and provide the best separation between the two classes [16]. This method is efficient in that it uses the histogram of the corresponding node distances to compute the threshold. In this investigation Otsu's method is implemented to locate the maximum between-class variance of the histogram data from the corresponding distances between the stereophotogrammetry and CT nodes.

In Otsu's method let *{0, 1, 2, ..., L-1}* denote the distinct bins of corresponding distance levels from the registered

(a) Plastic head

(d) Polystyrene head
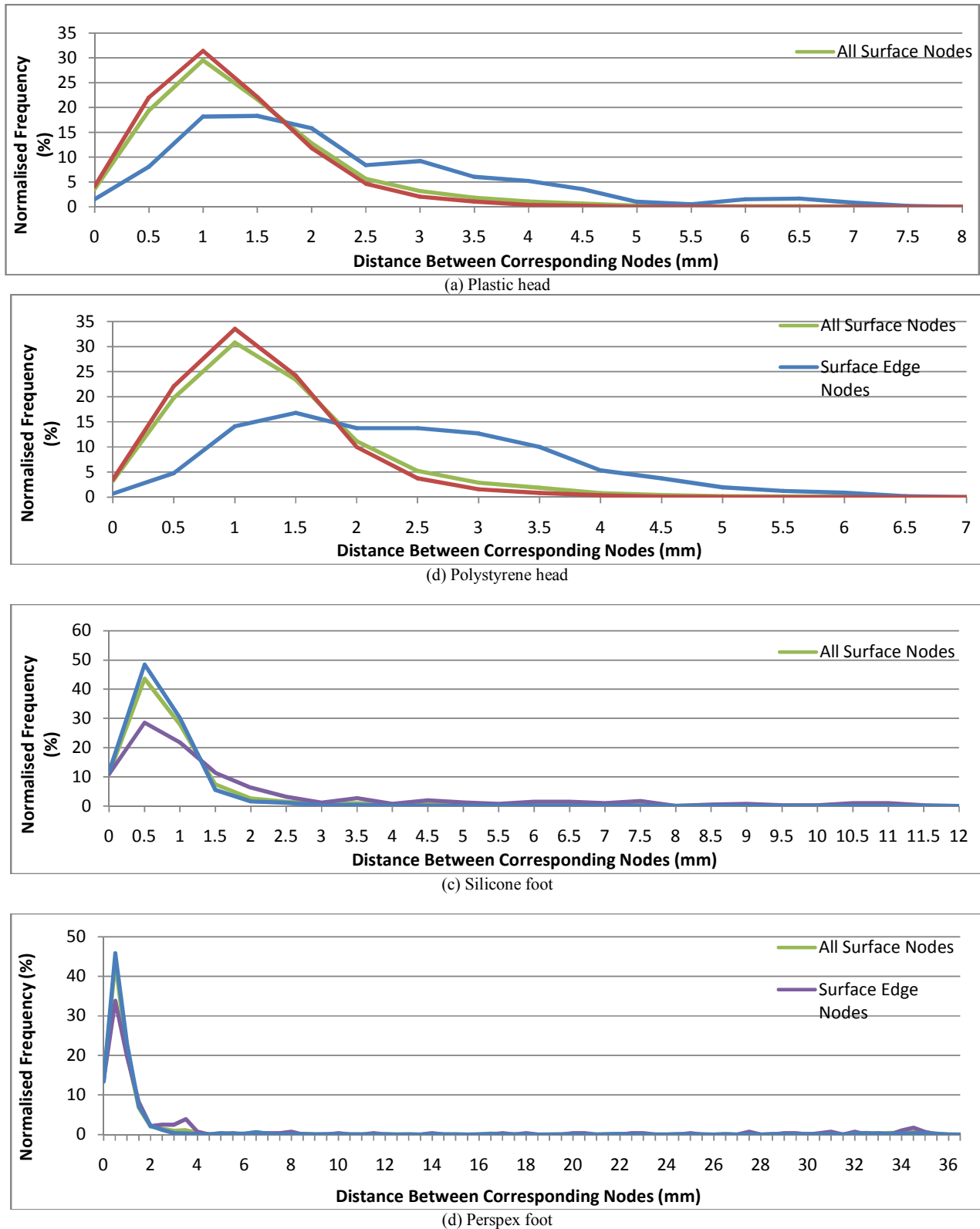

(c) Silicone foot

(d) Perspex foot

Fig. 4 The normalized distribution of corresponding node distance between the stereophotogrammetry surface nodes and the closest CT surface nodes for (a) polystyrene head; (b) plastic head; (c) silicone foot; (d) Perspex foot;

stereophotogrammetry and CT data. The number of corresponding distances n_i denotes the number of stereophotogrammetry nodes that have a corresponding CT node distance of i. The total number of stereophotogrammetry nodes in the surface is N. Therefore the normalized histogram uses p_i, the proportion of nodes at distance levels i.

$$p_i = n_i / N \qquad (1)$$

$$\sum_{i=0}^{L-1} p_i = 1, \; p_i \geq 0 \qquad (2)$$

From this data the aim of Otsu's algorithm is to find the distance threshold that maximizes between-class variance of two distance classes (inliers and outliers). The summary of the algorithm is as follows:

1) Compute the normalized histogram using p_i

$$p_i, \; i = 0,1,2,...,L-1 \qquad (3)$$

2) Determine the cumulative sums, $P_1(k)$ for $k = 0, 1, 2,..., L-1$

$$P_1(k) = \sum_{i=0}^{k} p_i \qquad (4)$$

3) Calculate the cumulative means, $m(k)$, for the thresholds $k = 0, 1, 2,..., L-1$.

$$m(k) = \sum_{i=0}^{k} ip_i \qquad (5)$$

4) Determine the global distance mean, m_G

$$m_G = \sum_{i=0}^{L-1} ip_i \qquad (6)$$

5) For each threshold $k = 0, 1, 2,..., L-1$, compute the between-class variance σ^2_B

$$\sigma^2_B(k) = \frac{[m_G P_1(k) - m(k)]^2}{P_1(k)[1 - P_1(k)]} \qquad (7)$$

6) Otsu's threshold, k^*, is the value of k which produces the maximum σ^2_B, (8). If a non-unique maximum is found, k^* is calculated as the average of the maxima located.

$$\sigma^2_B(k^*) = \max_{0 \leq k \leq L-1} \sigma^2_B(k) \qquad (8)$$

Therefore to find the optimal threshold using Otsu's algorithm, all the binned distance values in the normalized histogram are used and (8) is evaluated. The value of k that produces the maximum in (8) is then selected as the threshold unless more than one maximum exists. If more than one maximum is found the values of k that produces these maxima values are averaged [16].

2) Mean and Standard Deviation of Corresponding Stereophotogrammetry and CT Distance

The second method used to determine outliers, using the corresponding stereophotogrammetry to CT distance, are with the mean and standard deviation (SD) of the corresponding distance nodes. Let $i = \{0, 1, 2,...,n-1\}$ be the index of each node in the stereophotogrammetry surface with N nodes. Each stereophotogrammetry node has a distance to its closest CT node of d_i. From the normalized histograms in Fig. 4 the mean

and standard deviation of corresponding distance can be calculated. By using all the corresponding distance values the mean, (μ), and standard deviation, (σ), can be sought and different combinations of the mean and standard deviations tested. In this investigation the threshold was selected based on variations of $\mu + \alpha\,\sigma$, where $\alpha = 1, 1.5, 2$.

$$\mu = \frac{1}{N} \sum_{i=0}^{n-1} d_i \qquad (9)$$

$$\sigma = \sqrt{\frac{1}{N} \sum_{i=0}^{n-1} (d_i - \mu)^2} \qquad (10)$$

3) Data Cleansing Algorithms

In this investigation the following cleansing algorithm is used with the registered stereophotogrammetry and CT surfaces for all the phantoms in Fig 1. The algorithm finds the distance threshold and the nodes on the stereophotogrammetry surface edge that have a distance equal to or greater than this threshold.

The iterative automated data cleansing algorithm is as follows:

Automated Stereophotogrammetry Data Cleansing Algorithm	
Input:	Stereophotogrammetry 3D surface mesh (SPG)
	CT 3D surface mesh (CT)
	Change in RMS distance threshold (RMS$_{thresh}$)
Output:	Cleansed stereophotogrammetry surface
1 **begin**	
2	find closest CT node for every SPG node
3	calculate the distance d_i between each SPG node and its closest CT node
4	Calculate the root mean square (RMS) of corresponding node distance for every SPG node
	$$RMS_{curr} = \sqrt{\frac{1}{N} \sum_{i=0}^{n-1} d_i^2}$$
5 **while**(RMS$_{thresh}$ < RMS$_{change}$)	
6	find the distance threshold T using all the corresponding distance values d_i with either Otsu's or mean plus SD ($\mu + \alpha\,\sigma$) approach
7	find the nodes on the SPG surface edge
8	find which SPG surface edge nodes have a distance, d_i, $\geq T$, these nodes become outliers
9	remove outlier nodes from SPG surface that do not cause surface disjoint
10	RMS$_{prev}$ = RMS$_{curr}$
11	calculate the RMS$_{curr}$ for the cleansed SPF surface
12	RMS$_{change}$ = RMS$_{prev}$ - RMS$_{curr}$
13 **endwhile**	
14 **end**	

A disjoint detection algorithm was implemented to test which outlier nodes could be successfully removed without causing the stereophotogrammetry surface from becoming disjointed. Ideally all the surface edge nodes that meet the

threshold criteria would be removed. However if these nodes were removed a scenario could occur where the surface becomes disjointed, meaning that there could be clusters of nodes and facets that would not be connected to the main surface. Consider the sub surface in Fig. 5, where surface edge nodes 34 and 40 had a corresponding distance ≥ to the distance threshold. If node 34 was only to be removed, then facets F37, F38, F41, F42 and F43 would no longer exist. No disjoint would occur since node 41 connects facets F52 and F44. Likewise, if node 40 was to be removed, facets F44, F45 and F49 would be removed and no disjoint would occur since node 35 connects facets F43 and F46. However, when both nodes 34 and 40 are removed, facets F37, F38, F41, F42, F43, F44, F45 and F49 are removed. Therefore, facets F46, F47 and F48 are no longer connected to the main surface and a disjoint occurs.
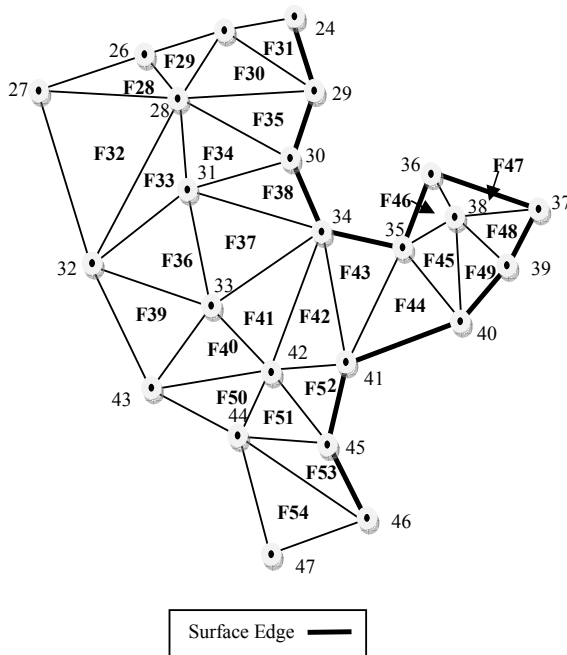

Fig. 5 The sub surface of a mesh where the removal of surface edge nodes creates a disjointed surface

In this work automatic selection of thresholds were investigated using the corresponding distances of every stereophotogrammetry surface node and its closest node in the CT surface:
1) Otsu's method
2) Mean and standard deviation variants, $\mu + \alpha \sigma$, where $\alpha = 1, 1.5, 2$

This algorithm was applied to the registered stereophotogrammetry and CT data for the silicone foot, Perspex foot, polystyrene head and plastic head. Corresponding node distance bins of 0.1mm were used, with the terminating change in RMS set to 0.001mm. Both threshold types were investigated, however the mean and standard deviation thresholds were independently tested at (a) mean + 1SD; (b) mean + 1.5SD; (c) mean + 2SD.

At each iteration the distance threshold (mm), number of surface edge nodes that meet the threshold criteria, number of surface edge nodes removed (without causing surface disjoint) and new distance RMS between the two surfaces is recorded. Furthermore for each iteration both the frequency and normalized frequency of the corresponding distance values for the entire stereophotogrammetry surface nodes, surface edge nodes (level 1), level 2 nodes, level 3 nodes and the remaining nodes are recorded.

III. RESULTS

Each algorithm was applied to the registered stereophotogrammetry data acquired from the 4 phantoms, plastic radiography head; the silicone foot; Perspex foot; and Polystyrene head.

A. Plastic Head Phantom

For each of the algorithms tested, the cleansing of the stereophotogrammetry surface of the plastic head removed many regions of outliers along the surface edge. The cleansing algorithm using Otsu's method produced an overall improvement in RMS, 0.37mm (Table I). The first iteration had a threshold of 2.1mm, which then fluctuated between 1.7mm and 1.8mm for the remaining iterations. This threshold had no gradual decline unlike the mean and SD approaches. After several iterations, there are clusters of data that are connected to the main surface by only a few nodes which caused a high number of nodes to be located, but only a small proportion of these nodes to be removed as a disjoint would have occurred. This is further reflected in that the change in RMS after 9 iterations falls to below 0.01mm. However, this approach provides an unusable cleansed surface with large regions in the forehead, chin and neck removed (Fig. 6(b)). These regions have clusters of nodes that are connected to the main surface by a line of nodes which cannot be removed as a surface disjoint would occur.

TABLE I
PLASTIC HEAD: AUTOMATIC DATA CLEANSING RESULTS

	Otsu	Mean + SD	Mean + 1.5SD	Mean + 2SD
Number of Iterations	19	7	6	6
Number of Surface Edge Nodes Removed	1514	654	464	346
Start RMS (mm)	1.87	1.87	1.87	1.87
End RMS (mm)	1.50	1.62	1.65	1.67
RMS Improvement (mm)	0.37	0.25	0.22	0.2
Final Threshold (mm)	1.8	2.16	2.53	2.93

With the mean and 1SD as the cleansing threshold, the overall RMS improvement is 0.25mm (Table I). From the 1st iteration to the 4th iteration the change in the threshold value declines by at least 0.1mm, producing a change in RMS of >0.1mm. On visual inspection of the cleansed stereophotogrammetry surface, it is evident that the outliers around the surface edge have been removed (Fig. 6(c)). However several node clusters have been removed just below one of the eyes and near the ear region.

The mean plus 1.5SD improves the RMS 0.22mm (Table I). The distance thresholds set by this approach, started at

2.99mm, finishing at 2.53mm. After 4 iterations the change in the distance threshold falls to < 0.01mm, which impacts the change in RMS between iterations to <0.001mm. When this occurs very few surface edge nodes are located and removed. The visual inspection of the surface cleansed with this approach is a good visualization, Fig. 6(d), since much of the surface edge is removed from the entire surface, but regions of anatomical significance have been kept.

The mean plus 2SD approach produces an improvement in RMS of 0.2mm (Table I). This method distance thresholds starting at 3.43mm and ending at 2.93mm. The high threshold limits set using this method creates a scenario that detects few nodes after 4 iterations that meets the threshold criteria. After 4 iterations the change in the distance threshold is <0.01mm impacting on the RMS change so that it is <0.01mm. The visualization of the surface created by this cleansing approach shows that little of the surface edge data has been removed from the surface and there are areas around the surface edge that no data has been removed (Fig. 6(e)).
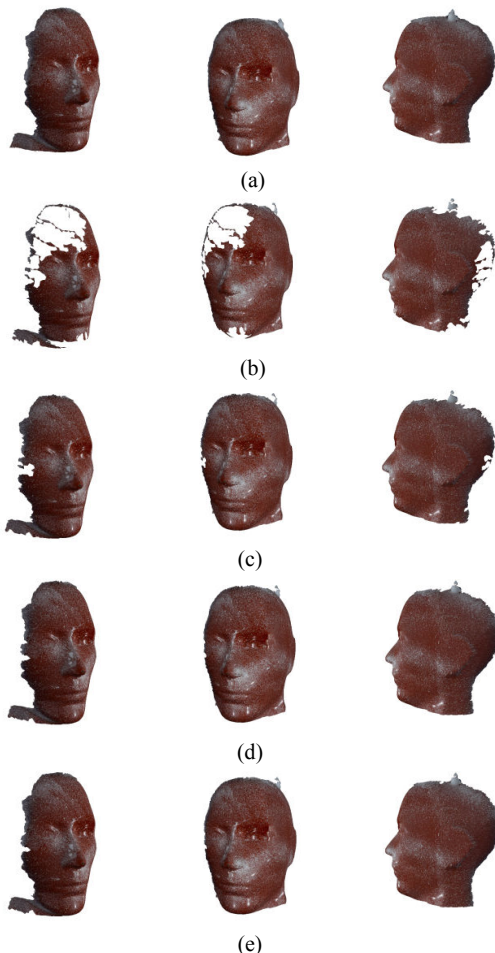

(a)

(b)

(c)

(d)

(e)

Fig. 6 Profiles of the stereophotogrammetry plastic head surface (a) prior to cleansing; (b) with Otsu cleansing; (c) mean + SD; (d) mean + 1.5SD; (e) mean + 2SD

From the normalized distribution of corresponding distances the Otsu based approach has a maximum normalized distribution of 7.92% at 1.1mm compared non-cleaned data

having a maximum distribution of 6.22% at 1mm (Fig. 7). The mean plus 1SD, 1.5 and 2SD all have a maximum distribution at 1mm with 6.86%, 6.66% and 6.55% respectively. The normalized distribution of nodes that have a corresponding distance of <2mm, using Otsu's method is 87.95% compared with the original surface having 74.15% prior to cleansing. The normalized distribution for this corresponding distance range with the mean plus 1SD, 1.5SD and 2SD is 81.69%, 79.35% and 77.96% respectively.
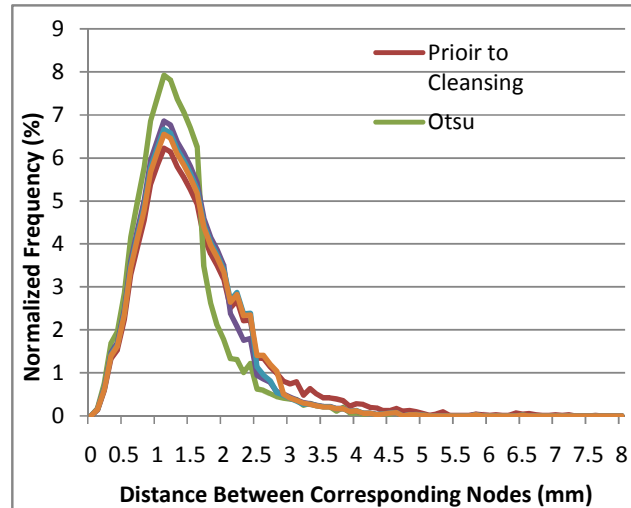

Fig. 7 The normalized frequency distribution of corresponding distances for the plastic head stereophotogrammetry surface prior to cleansing and for all the algorithms implemented

B. Silicone Foot Phantom

The results from cleansing the silicone foot stereophotogrammetry surface are outlined in Table II. Using Otsu's method the RMS was improved from 1.84mm to 1.04mm, an improvement of 0.80mm. The distance threshold set by this approach starts at 3.7mm and decreases to 0.9mm after 9 iterations. This threshold remains at 0.9mm for the remaining 19 iterations, and with such a low corresponding distance threshold a large amount of nodes are removed until termination. After the 9th iteration the number of nodes that meet the threshold criteria are high but less than half of these detected are removed. This is due to clusters of nodes being connected to the main surface by only a few nodes. Removal of these connecting nodes would have caused a surface disjoint, and so were not removed.

The cleansing of the stereophotogrammetry surface using Otsu's method created a surface with large regions of important data removed (Fig.8 (b)). This included the heel, arch and metatarsal heads (where the two ulcers are located). The mean plus 1SD approach removed areas around the toes and a significant portion of the inner arch region (Fig.8 (c)). With the mean plus 1.5SD nodes around the entire surface edge are removed, but the internal data remains (Fig 8(d)). Little data is removed from around the surface edge with the mean plus 2SD (Fig 8(e)).

Examination of the normalized frequency distribution of the corresponding distances for all stereophotogrammetry surface

nodes, Fig. 9, shows that prior to cleansing 90.08% of all the surface nodes had a corresponding distance of <2mm. The proportion of nodes within a corresponding distance of <2mm for using Otsu, mean plus 1SD, mean plus 1.5SD and mean plus 2SD are 90.08%, 99.71%, 99.08%, 99.02% and 99.01% respectively.

TABLE II
SILICONE FOOT: AUTOMATIC DATA CLEANSING RESULTS

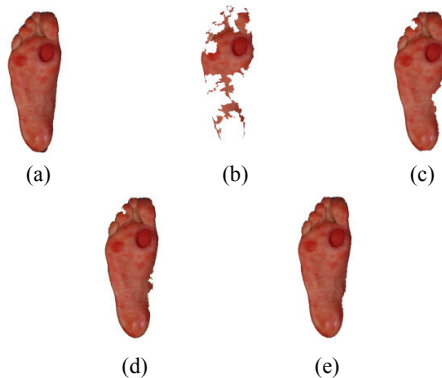|	Otsu	Mean + SD	Mean + 1.5SD	Mean + 2SD
Number of Iterations	28	11	11	10
Number of Surface Edge Nodes Removed	1427	550	401	333
Start RMS (mm)	1.84	1.84	1.84	1.84
End RMS (mm)	0.80	0.95	0.99	1.01
RMS Improvement (mm)	1.04	0.89	0.85	0.83
Final Threshold (mm)	0.9	1.24	1.49	1.72

(a)   (b)   (c)

(d)   (e)

Fig. 8 The stereophotogrammetry silicone foot surface (a) prior to cleansing; (b) with Otsu cleansing; (c) mean + SD;
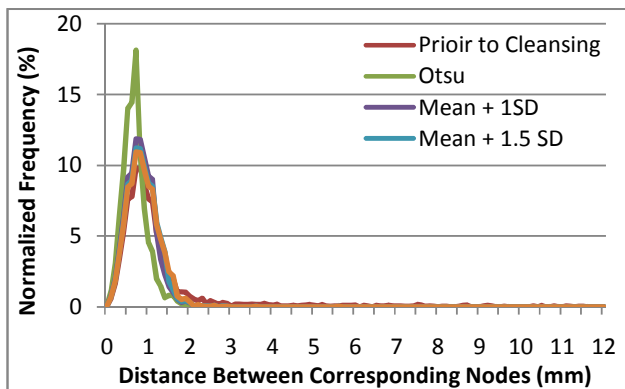(d) mean + 1.5SD; (e) mean + 2SD

Fig. 9 The normalized frequency distribution of corresponding distances for the silicone foot stereophotogrammetry surface prior to cleansing and for all the algorithms implemented

C. Perspex Foot

On visual inspection of the Perspex foot prior to cleansing a large artifact was visible on the RHS of the ankle region at the end of the field of view of the cameras. The returned RMS from cleansing the surface from all approaches is still high in the region of 4.37mm-4.85mm (Table III). On visual inspection of the surfaces the all of the algorithms failed to

remove this large artifact and subsequently any outliers around the rest of the phantom's surface edge (Fig. 10). This shows that these approaches are not suitable for removing large artifact data before cleansing the rest of the surface edge. Post-cleansing all the returned surface data had stereophotogrammetry nodes with a maximum distance of 36.2mm.

TABLE III
PERSPEX FOOT: AUTOMATIC DATA CLEANSING RESULTS

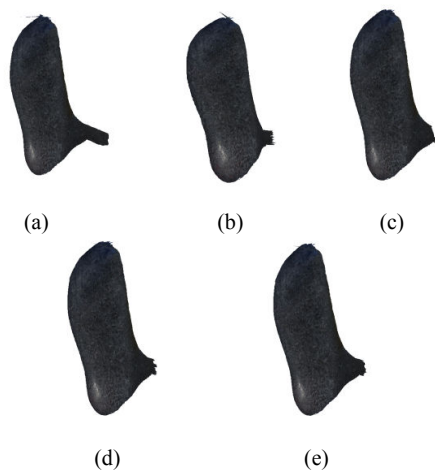|	Otsu	Mean + SD	Mean + 1.5SD	Mean + 2SD
Number of Iterations	8	10	8	8
Number of Surface Edge Nodes Removed	160	215	180	170
Start RMS (mm)	7.8	7.8	7.8	7.8
End RMS (mm)	4.85	4.37	4.79	4.82
RMS Improvement (mm)	2.95	3.43	3.01	2.98
Final Threshold (mm)	14.2	5.67	8.44	10.73

(a)   (b)   (c)

(d)   (e)

Fig. 10 The stereophotogrammetry Perspex foot surface (a) prior to cleansing; (b) with Otsu cleansing; (c) mean + SD;
(d) mean + 1.5SD; (e) mean + 2SD

D. Polystyrene Head

The stereophotogrammetry data of the polystyrene head had a lot of small artifacts around the surface edge, especially around the surface edge of the head. All the algorithms tested were successful in removing outlier regions such as these with varying levels of success. Otsu's method returns an RMS of distance improvement of 0.3mm (Table IV). The mean plus 1SD, 1.5SD and 2SD yield an RMS improvement of 0.24mm, 0.21mm and 0.18mm respectively. The distance threshold set by Otsu's method at the first iteration is 2mm which is less than the other methods. This distance threshold set by Otsu's method is lowered to 1.6mm after 4 iterations and remains at this distance threshold until the algorithm terminates. This means that the fewer nodes are removed and the change in RMS at each iteration is <0.001mm.

The visual inspection of the cleansed surfaces shows that a large amount of useful data around the ears, temples and the forehead (Fig. 11(b)). With the mean plus 1SD approach important anatomical data around the ears is removed. The mean plus 1.5SD removes nodes from the surface edge but does not remove internal surface areas (Fig. 11(c)). In

comparison with the surface prior to cleansing, Fig. 11(a), little of the surface edge data is removed using the mean plus 2SD in Fig. 11(e).

TABLE IV
POLYSTYRENE HEAD: AUTOMATIC DATA CLEANSING RESULTS

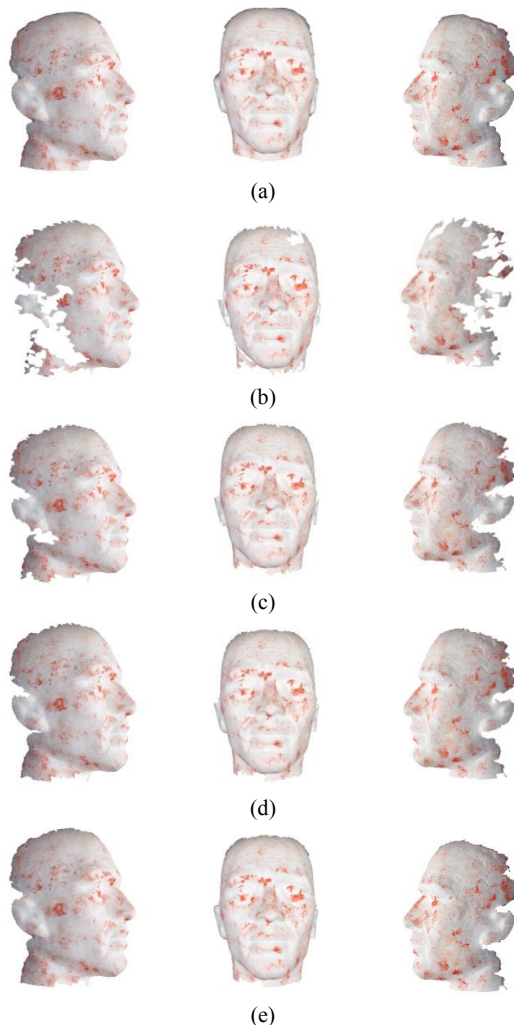|	Otsu	Mean + SD	Mean + 1.5SD	Mean + 2SD
Number of Iterations	24	12	9	8
Number of Surface Edge Nodes Removed	1486	828	591	412
Start RMS (mm)	1.79	1.79	1.79	1.79
End RMS (mm)	1.49	1.55	1.58	1.61
RMS Improvement (mm)	0.3	0.24	0.21	0.18
Final Threshold (mm)	1.6	2.05	2.41	2.78

(a)

(b)

(c)

(d)

(e)

Fig. 11 Profiles of the stereophotogrammetry polystyrene head surface (a) prior to cleansing; (b) with Otsu cleansing; (c) mean + SD; (d) mean + 1.5SD; (e) mean + 2SD

The normalized distribution of the corresponding node distances for the stereophotogrammetry surface shows the effect that the cleansing has on the improvement to the corresponding distances (Fig. 12). From the distribution data the stereophotogrammetry surface has 77.21% of its nodes

with a corresponding distance of <2mm. Using Otsu's method in cleansing the distribution of corresponding node distances of <2mm is 88.25%. The mean plus SD cleanses the surface so that 86.03% of the nodes have a corresponding distance within 2mm. With the mean plus 1.5SD this distribution is 83.31% and for the mean plus 2SD the proportion of nodes in the range is 81.36%.
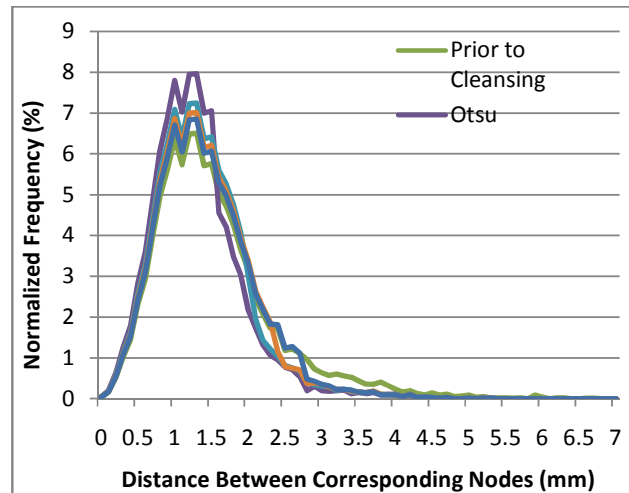

Fig. 12 The normalized frequency distribution of corresponding distances for the polystyrene head stereophotogrammetry surface prior to cleansing and for all the algorithms implemented

IV. DISCUSSION

The cleansing of the plastic head shows the stereophotogrammetry surface can return a good improvement in the RMS distance between the two surfaces and increase the distribution of nodes with a corresponding distance of 2mm. Although Otsu's method yielded the best RMS improvement, 0.37mm, large areas of the surface including the forehead, chin and neck were removed (Fig. 6(b)). This shows that the greatest RMS improvement does not guarantee that the visualized surface will not have important areas of surface removed. Although the mean plus 1.5SD yields the best visualization, Fig. 6(d), this method does not return the best improvement in RMS, the highest number of nodes removed or the best normalized corresponding distance distribution (Table I and Fig. 7). This approach removed surface edge outliers around the entire surface edge without removing more internal data, making this cleansing approach the most suitable cleansing mechanism for visualization.

The results from cleansing the silicone foot show that Otsu's approach returns the greatest RMS improvement compared with the other methods (Table II). In comparing the normalized distributions of the 4 algorithms, the Otsu based approach yields a greater maximum distribution (Fig. 9). However this approach does not produce a clinically usable surface with many regions of anatomical significance removed. The reason for this is that the distance threshold to identify outliers is considerably lower than the other methods. The mean plus 1.5SD method returns the most usable surface data with outliers from the surface edge removed from around the entire surface (Fig. 8(d)). This method returns a distance

threshold at each iteration which prevents the removal of large proportions of the surface edge.

Cleansing of the Perspex foot was unsuccessful as a result of a large artifact in the ankle region. All the algorithms failed to remove this artifact or any other outlier data from the rest of the stereophotogrammetry surface edge (Fig. 10). This failure to remove this artifact would cause misinterpretation of the surface data. All cleansed stereophotogrammetry surfaces had corresponding distances of 36.2mm. This shows that more work is required in removing large artifacts so that the remainder of the surface edge can be cleansed.

The results from the polystyrene head shows that the difference in RMS improvement is small between each method, but the difference in the number of nodes removed for this gain is very high. The method that uses the mean plus 1.5SD produces the best visualization, with a clinically acceptable amount of nodes removed. This method does not have the best RMS improvement or the best normalized distribution (Table IV, Fig.12). However, the overall visualization of the surface is the most appropriate, with areas of importance kept, but a substantial amount of surface edge outlier removed (Fig 11(d)).

With the use of automated cleansing algorithms the overall RMS between the two surfaces can be improved by iteratively setting a distance threshold and finding surface edge nodes with a corresponding distance that meets the threshold criteria. Over all the surfaces Otsu's approach produced the lowest thresholds, except for the Perspex foot phantom. As a result of this a lot of data was removed with data removed that was in areas of clinical significance producing the lowest RMS and the removing the highest number of nodes. The distance thresholds with Otsu's approach did not decrease at each iteration unlike the mean and SD approaches.

The findings from the Perspex foot showed that each approach cannot remove large artifacts in the examples provided since the stereophotogrammetry data that has no corresponding CT data in this region. This yields high corresponding distances, which in turn produce high distance thresholds so that few surface edge nodes are removed. Furthermore, with this data the algorithms did not remove any surface nodes from the rest of the surface and produced high RMS values post-cleansing. This highlights that further work is required in adapting the algorithms to highlight and remove these large artifact areas.

Therefore in choosing one of these algorithms to automatically cleanse stereophotogrammetry data, careful consideration must be given to the tradeoff between the RMS improvement and the visualization of the cleansed surface. Further work is required in selecting a better termination condition for these approaches so that an appropriate amount of data is removed for an acceptable RMS improvement. Stereophotogrammetry data is captured with the cameras focused in the centre of the region of anatomical importance. Therefore the algorithms could be adapted to ignore the removal of surface nodes near the central capture region.

V. CONCLUSION

This investigation has shown that there is a high distribution of outliers in and around the surface edge of stereophotogrammetry data and these can be automatically removed. However these approaches require refinement to remove large artifacts and surface edge outliers without removing clinically significant data. Future work will focus on improving the data cleansing, so that large artifacts and outlier on the surface edge are removed, without removing areas of clinical significance. This work is part of a framework for automated visualization of stereophotogrammetry and CT data. As part of this process the stereophotogrammetry data requires cleansing to remove outliers and artifacts which can produce a poor representation of the surface and limits the misinterpretation of this data.

REFERENCES

[1] J. K. Iglehart, "The new era of medical imaging progress and pitfalls," *New England Journal of Medicine*, vol. 354, no. 26, pp. 2822-2828, 2006.

[2] C. Studholme, D. L. Hill, and D. J. Hawkes, "Automated 3-D registration of MR and CT images of the head.," *Medical image analysis*, vol. 1, no. 2, pp. 163-75, Jun. 1996.

[3] Winder RJ, Darvan T, McKnight W, Magee J, Ramsay-Baggs P. Technical validation of the Di3D stereophotogrammetry surface imaging system. British Journal of Oral and Maxillofacial Surgery 2008, 46, 33-37.

[4] S. K. Williams, L. a Ellis, and G. Williams, "A 3D digital medical photography system in paediatric medicine." *Journal of visual communication in medicine*, vol. 31, no. 3, pp. 91-8, Jan. 2008.

[5] T. J. J. Maal, J. M. Plooij, F. a Rangel, W. Mollemans, F. a C. Schutyser, and S. J. Bergé, "The accuracy of matching three-dimensional photographs with skin surfaces derived from cone-beam computed tomography.," *International journal of oral and maxillofacial surgery*, vol. 37, no. 7, pp. 641-6, Jul. 2008.

[6] R. Dirnhofer, C. Jackowski, P. Vock, K. Potter, and M. J. Thali, "VIRTOPSY: minimally invasive, imaging-guided virtual autopsy.," *Radiographics: a review publication of the Radiological Society of North America, Inc*, vol. 26, no. 5, pp. 1305-33, 2006.

[7] J. M. Riphagen, J. W. van Neck, and L. N. a van Adrichem, "3D surface imaging in medicine: a review of working principles and implications for imaging the unsedated child.," *The Journal of craniofacial surgery*, vol. 19, no. 2, pp. 517-24, Mar. 2008.

[8] J. P. Siebert and S. J. Marshall, "Human body 3D imaging by speckle texture projection photogrammetry," *Sensor Review*, vol. 20, no. 3, pp. 218-226, 2000.

[9] W. E. Lorensen and H. E. Cline, "Marching cubes: A high resolution 3D surface construction algorithm," in *Proceedings of the 14th annual conference on Computer graphics and interactive techniques*, 1987, pp. 163–169.

[10] R. A. Robb, "The biomedical imaging resource at Mayo Clinic," *IEEE Transactions on Medical Imaging*, vol. 20, no. 9, pp. 854-867, 2001.

[11] J. Murray and W. Van Ryper, "Wavefront OBJ File Format Summary," 2005. [Online]. Available: http://www.fileformat.info/format/wavefrontobj/egff.htm. [Accessed: 01-Jun-2012].

[12] P. Cignoni, M. Callieri, M. Corsini, F. Ganovelli, and G. Ranzuglia, "Meshlab Visual Computing Lab - ISTI - CNR," 2010. [Online]. Available: http://meshlab.sourceforge.net/.

[13] D. Chetverikov, D. Svirko, D. Stepanov, and P. Krsek, "The trimmed iterative closest point algorithm," in *International Conference on Pattern Recognition*, 2002, vol. 16, pp. 545-548.

[14] S. Henry, P. Morrow, J. Winder, and B. Scotney, "ICP Variants Robustness to Gaussian and Impulsive Noise," in *16th Conference on Medical Image Understanding and Analysis*, 2012, pp. 1-6.

[15] N. Otsu, "A threshold selection method from gray-level histograms," *IEEE Transactions on Systems, Man and Cybernetics*, vol. 20, no. 1, pp. 62-66, 1979.

[16] R. C. Gonzalez and R. E. Woods, "Digital image processing," in *Digital image processing*, 3rd ed., Prentice Hall, 2008, pp. 742-747.